9-5-2019

Composition of Templates for Transitional Pedipulation Behaviors

Thomas T. Topping
University of Pennsylvania, ttopping@seas.upenn.edu

Vasileios Vasilopoulos
University of Pennsylvania, vvasilo@seas.upenn.edu

Avik De
Harvard University, avikde@seas.harvard.edu

Daniel E. Koditschek
University of Pennsylvania, kod@seas.upenn.edu

Composition of Templates for Transitional Pedipulation Behaviors

Abstract

Abstract. We document the reliably repeatable dynamical mounting and dismounting of wheeled stools and carts, and of fixed ledges, by the Minitaur robot. Because these tasks span a range of length scales that preclude quasi-static execution, we use a hybrid dynamical systems framework to variously compose and thereby systematically reuse a small lexicon of templates (low degree of freedom behavioral primitives). The resulting behaviors comprise the key competences beyond mere locomotion required for robust implementation on a legged mobile manipulator of a simple version of the warehouseman's problem.

Disciplines

Electrical and Computer Engineering | Engineering | Systems Engineering

Composition of Templates for Transitional Pedipulation Behaviors

T. Turner Topping[1], Vasileios Vasilopoulos[2], Avik De[3], Daniel E. Koditschek[1]

[1] T. Turner Topping and Daniel E. Koditschek are with the Department of Electrical and Systems Engineering, University of Pennsylvania, Philadelphia, PA 19104, {ttopping,kod}@seas.upenn.edu

[2] Vasileios Vasilopoulos is with the Department of Mechanical Engineering and Applied Mechanics, University of Pennsylvania, Philadelphia, PA 19104, vvasilo@seas.upenn.edu

[3] Avik De is with the School of Engineering and Applied Sciences, Harvard University, Cambridge, MA 02138, avikde@seas.harvard.edu

Abstract. We document the reliably repeatable dynamical mounting and dismounting of wheeled stools and carts, and of fixed ledges, by the Minitaur robot. Because these tasks span a range of length scales that preclude quasi-static execution, we use a hybrid dynamical systems framework to variously compose and thereby systematically reuse a small lexicon of templates (low degree of freedom behavioral primitives). The resulting behaviors comprise the key competences beyond mere locomotion required for robust implementation on a legged mobile manipulator of a simple version of the warehouseman's problem.

1 Introduction

Autonomously rearranging the configuration of furniture in a cluttered room is an algorithmically hard problem [1] for which simpler instances can be addressed by recourse to appropriate abstraction [2]. Suitably coupling such an abstract (offline) task planner with a runtime reactive motion planner [3] has permitted empirical rearrangement of wheeled stools and carts in the physical world [4] by a mobile manipulator [5] whose reliance on legs earns its behavior the term "pedipulation" [6]. In [4], mobility to and of these objects was achieved by previously developed robust (asymptotically stable) closed loop locomotion and pushing gaits. In contrast, because these objects dwarf the robot and have caster-wheeled bases that will spin away if poorly engaged, the messy details of "grasping" — mounting into and then dismounting to release from their force-closure graspable surfaces — was left to the case-by-case provision of an open loop transition scheme developed by human intuition, resulting in a fragile implementation, each of whose instances typically required numerous re-takes to achieve. In this paper, we present empirical evidence that these delicate grasping tasks, comprising the key pedipulation competences required for robust success of this approach beyond mere mobility, can be specified and executed by recourse to further abstraction that anchors a lexicon of low degree of freedom

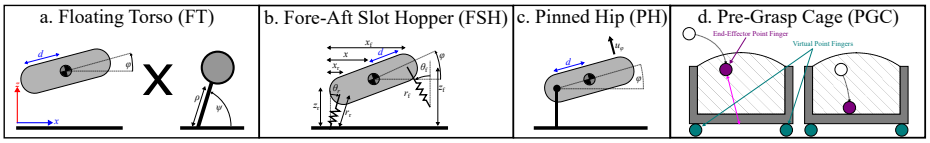

Fig. 1. The primary template models used to compose the behaviors in this paper.

closed loop dynamical templates [7], (depicted in Fig. 1) in the high degree of freedom Minitaur robot [8, 9], whose systematic parallel and sequential compositions yield the full range of necessary grasping behaviors in a rational, robust, highly repeatable and reliable manner.

1.1 Related Literature

A large, longstanding [11] and still very active [12, 13] literature concerns the design and control of legged robots equipped with additional arms (and, not infrequently, wheeled legs [14]) for purposes of mobile manipulation, typically focusing on quasi-statically formed grasps and movements. Notwithstanding their similar engagement with manipulators mounted on legs, the focus of [15] on composition of simple primitives comes closer to our work, but does not address the problem of scale mismatch which we believe is a crucial barrier to increasing the utility of small, cheap robots in human scale settings. The smaller but similarly longstanding [6] literature on dynamical pedipulation appears to focus even in recent years on impulsive interaction with the movable objects [16] including, seemingly most close to our work, a recent simulation study on repeated, constrained, impulsive pushes for controlled ball rolling [17]. In contrast, we seek dynamically formed force closure grasps for purposes of pushed or dragged rearrangement [4] in the physical world.

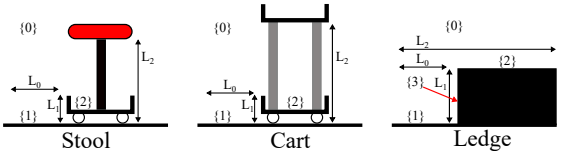

Common Contact Modes	
Aerial (A)	(0,0)
Single Support, Ground (SSG)	(1,0)
Double Support, Ground (DSG)	(1,1)
Double Support, Split (DSS)	(1,2)
Double Support, Ledge (DSL)	(2,2)

Fig. 2. A depiction of the different task-environments used, and their intrinsic parameters, $L_i, i \in \{0, 1, 2\}$. The horizontal distances, L_0 in all three environments and L_2 in the ledge environment, denote the initial standoff of the distal toe in modes $(1, j)$ and $(j, 1)$ for $j \in \{0, 1, 2\}$. The numbers in brackets ($\{\cdot\}$) label that surface's contact mode when a limb is in contact with it, and we adopt the notation of [10] to denote the cells of the resulting ground reaction complex (GRC) by ordered pairs of contact labels whose first slot denotes the contact condition of the left toe and whose second slot the right.

Because these varied situations admit the possibility of collision (undesired contacts between the robot's body and the object to be pedipulated prior to the designated toe-grasp) we make repeated use of templates emerging from work in progress that use parallel composition of still simpler constituent templates to approximately decouple body attitude from either height (floating torso [18]: FT, Fig.1a) or proximity (fore-aft slot-hopper [19]: FSH, Fig. 1b). This greatly facilitates leap sequences that require clearing the lower lip while not grazing the upper shelf of the stool or cart while achieving mounts, dismounts and leaps that land normal to the escape-prone stools and carts.[4] Although still human generated for purposes of this paper, we aim to drive this new lexicon of parametrized controllers from higher level planners such as the reactive layer of [4], to be placed at the command of fully symbolic task planners such as described in [2, 24].

1.2 Contributions and Organization of the Paper

We document the reliably repeatable dynamical mounting (Figs. 6,7) and dismounting (Figs. 8,9) of wheeled stools and carts and fixed ledges (Figs. 10,11) using various sequential compositions of the templates depicted in Fig. 1 implemented on the Minitaur robot. After reviewing the constituent template models in Section 2, we describe in Section 3 the formal closed loop hybrid dynamical systems [25] — for mounting (Fig. 3), dismounting (Fig. 4), and leaping (Fig. 5) — resulting from the controllers applied to these template models and the guards triggering their hybrid switches. Section 4 concludes with a presentation of our empirical results, comprising the central contribution of the paper.

2 Template Models

We now describe our lexicon of templates, adjoining to the pre/post grasp parallel compositions (FT, Fig.1a [18]; and FSH, Fig.1b [19]) a simple "pinned hip" template (PH, Fig. 1c) (3) for injecting energy in a controlled manner. To initiate (or disengage from) the pushing behaviors documented in [4] we adopt a template-like approach to grasping by targeting a pre-grasp cage (PGC, Fig. 1d) terminating in (or initiated by) force closure grasps with real (the robot's toe) and virtual (the immobilizing floor)"point fingers" as inspired by [26]. The model anchor for all those dynamical primitives is the extended sagittal plane biped [27], whose configuration space, $\mathcal{Q} = (SE(2) \times \mathbb{R}^2 \times T^2)$, adds to the 3 DOF templates of Fig. 1 a pair of independently articulated legs — in coordinates, $q = (x, z, \phi, r_f, r_r, \theta_f, \theta_r) \in \mathcal{Q}$, where x is the horizontal position of the body COM, z is the vertical position of the COM, ϕ is the body pitch, r_f and r_r are the extensions of the front and rear legs respectively, and θ_f and θ_r are

[4] Because these models make relatively modest reasonable assumptions about the robot's body, we conjecture that this approach could be implemented on many different contemporary contemporary legged platforms, including but not limited to, the Ghost Vision [20], MIT Cheetah 3 [21], Agility Robotics Cassie [22], and Boston Dynamics Spot-Mini [23].

the leg angles of the front and rear legs relative to the body. However, a formal account of these template/anchor relations [7] lies beyond the scope of this paper which simply documents their empirical anchoring in the physical Minitaur robot through the plots of Section 4.

2.1 Floating Torso (FT)

The floating torso (FT) template [18] composes in parallel the dynamics of a sagittal inverted pendulum (i.e. a central-force accelerated planar point mass) essentially decoupled from planar body attitude dynamics as suggested in Fig. 1a, with dynamics taking the form

$$\begin{aligned} i_b\ddot{\phi} &= -k_P(\phi^* - \phi) - k_d\dot{\phi} \\ m_b\ddot{\rho} + G_p &= u_\rho - n_\theta + \mathcal{O}((\phi^* - \phi), \dot{\phi}) \end{aligned} \tag{1}$$

where i_b is the inertia of the body, ϕ is the pitch of the body, m_b is the mass of the body, and ρ is the extension of the virtual pendulum whose mass coincides with the body's COM when the pitching error terms, $\mathcal{O}((\phi^* - \phi), \dot{\phi})$, go to zero. Apart from the gravity-like term G_p, the central force acting on the extension of the point mass ρ is a virtual control input, u_ρ, representing the control affordance remaining after the attitude has been stabilized, opposed by "noise" terms, n_θ, from the virtual joint compliance associated with holding the desired physical posture that anchors the template, used here for facilitating pitch stable leaps.

2.2 Fore-Aft Slot Hopper (FSH)

Modeling the introduction of fore-aft dynamics to the slot-hopper template [27] as depicted in Fig. 1b is simplified [19] by assuming

1. The body pitch angle, ϕ is small, and $\sin(\phi) \approx \phi$.
2. The body length is sufficiently long so that inertial terms dominate the Coriolis/gravity terms.

Such a formulation approximates the position each hip, given by $\begin{bmatrix} x_{r/f} & z_{r/f} \end{bmatrix}^T = \begin{bmatrix} x & z \end{bmatrix}^T \pm d \begin{bmatrix} \cos(\phi) & \sin(\phi) \end{bmatrix}^T$ (where d is half the body length) as $\begin{bmatrix} x_{r/f} & z_{r/f} \end{bmatrix}^T \approx \begin{bmatrix} x & z \end{bmatrix}^T \pm d \begin{bmatrix} 1 & \phi \end{bmatrix}^T$, yielding the following dynamics in single stance:

$$\begin{aligned} \ddot{z}_r &= -gm_b\kappa + u_z\frac{m_b + 1}{m_b} - u_x\frac{(1+\kappa)x_r}{m_b\kappa\sqrt{x_r^2 + z_r^2}} + \mathcal{O}(\epsilon^2) \\ \ddot{z}_f &= -g + u_z\frac{1-\kappa}{m_b\kappa} + u_x\frac{(-1+\kappa)x_r}{m_b\kappa\sqrt{x_r^2 + z_r^2}} + \mathcal{O}(\epsilon^2) \\ \ddot{x}_r &= \frac{u_x}{m_b} + u_z\frac{x_r}{m_b\sqrt{x_r^2 + z_r^2}} + \mathcal{O}(\epsilon^2) \\ \ddot{x}_f &= \frac{u_x}{m_b} + \mathcal{O}(\epsilon^2) \end{aligned} \tag{2}$$

where m_b is the mass of the body, κ is the non-dimensional inertia [27], and $\mathcal{O}(\epsilon^2)$ represents higher order dynamics that can be treated as noise. Primarily, this work leverages the dynamics of the aerial hip in order to interact with objects, here denoted as $\ddot{x}_f$ and $\ddot{z}_f$. Furthermore, the horizontal dynamics of the front hip mimic those of the COM of the robot, which is useful when formulating controllers that require the front hip to clear obstacles in the xz plane.

2.3 Pinned-Hip Template (PH)

In many of the behaviors discussed, energy injection is required before transitioning into one of the templates described above. It is often convenient to anchor the platform to a pinned-hip template, where an arbitrary force can be applied to the body at the front hip, while the back leg maintains its extension and angle. As shown in Fig. 1c, this reveals a 1-DOF pendulum system in ϕ:

$$\ddot{\phi} = -\frac{g}{2d}\cos\phi + u_\phi \tag{3}$$

2.4 Pre-Grasp Cages (PGC)

While developing a generalized notion of grasping that is applicable to many "grippers" and many objects is difficult, the simplified notion of grasping [28] and caging [26] with point-contact fingers can be leveraged as an approximate template to which many robot morphologies can be anchored for purposes of pedipulation. This work assumes a virtual point "finger" resultant from the normal force applied to the object that remains fixed in the object's reference frame, and a movable finger, physically, the robot's "toe", which moves freely in $\mathbb{R}^2$. By ensuring that the pedipulator reaches a configuration where this "finger" can assert a squeezing cage [26], as depicted in Fig. 1d, we can ensure that the platform will maintain control of the object through landing, without disturbing the fore-aft position presumed by the offline deliberative planner of [3]. Conversely, by requiring, first, that the point-toe lift-off vertically and, next, escape the pre-grasp squeezing cage, we can ensure that the robotic platform will not disturb the erstwhile position prescribed by the offline deliberative planner [3] for the just previously manipulated object during dismounting tasks. While the geometry of each object determines the nature of its pre-grasp cage region, a careful analysis in the manner of [26] is required, and is outside the scope of this paper. Since this model lacks formal dynamics, we enforce the dynamics at the level of the anchor (simple P-D loops on the leg extensions and angles), and presume that there is adequate friction between both the "toe" and the object, as well as the "toe" and the ground.

3 A Selection of Mobile Manipulation Behaviors

3.1 Overview

The transitional behavior controllers formulated in this section are expressed as self-manipulation hybrid dynamical systems [25], where a system $\mathcal{H} = (\mathcal{I}, \Gamma, \mathcal{D},$

$\mathcal{F}$, $\mathcal{G}$, $\mathcal{R}$), is defined by a set of vertices ($\mathcal{I}$) and edges (Γ) of a graph defining transitions, a set of domains ($\mathcal{D}$) and dynamics ($\mathcal{F}$) indexed by each vertex and finally, a set of guard conditions ($\mathcal{G}$) and reset maps ($\mathcal{R}$) indexed by the edges.

Manipulating objects with a low degree of freedom robotic platform can be achieved in various ways; however, we focus on a legged analog of the dual differential drive convention defined in [5], where we assume that one pair of actuators (depicted as a single limb in the sagittal plane projection in Fig. 1b) is in contact with the ground and the second pair is manipulating an object of the kind depicted in Fig 2. Thus, we focus on the following class of "pedipulable" [6] objects, exemplified by the stool, cart and ledge of Fig. 2 each of which

1. possesses a feature or features on which a 2-DOF point "finger", in conjunction with a virtual point "finger" resultant from the normal force applied to the object by the ground, can produce a pre-grasp cage.
2. allows for a placement of the "gripper" toe into a grasp as described above.

3.2 Mounting Tasks

The mounting behavior, depicted in Fig. 3, is modeled as a sequence of three modes: a pitch-decoupled double-stance leap in mode DSG[5] or (1,1), ballistic flight (BF) in contact mode A or (0,0), and finally establishing a grasp on the object in the contact mode DSS or (1,2) thereby closing the pre-grasp cage. The goal of the behavior is to maneuver the free "finger" (in this case, the toe of the sagittal plane biped) into a squeezing cage configuration (see Section 2.4), while avoiding making contact with the object or with other parts of the body.

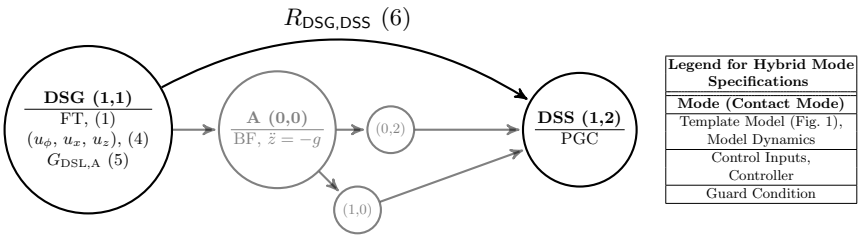

Fig. 3. A graph representing the hybrid dynamical system of the mount behavior. The gravity driven aerial phase (A) and subsequent single stance landing modes ({1,0} and {0,2}) can be integrated out and included in the reset map $R_{\text{DSG, DSS}}$.

Given a target object **O**, with sensed parameters $\{L_i\}_{i=0}^{2}$, an appropriate approach attitude $\phi \in [\phi_{min}, \phi_{max}]$ is selected, and from there, an appropriate

[5] The GRC "coordinates" (i.e., the pair of toe contact configurations) associated with this and the other mode name acronyms are presented in Fig. 2. In this initial paragraph we continue to list the GRC coordinates of the modes in alternation with their acronyms for reader's convenience.

ballistic trajectory for the platform's COM can be heuristically selected, subject to the specific concerns of the designer[6].

In mode DSG, we exploit the decoupling outlined in [18], utilizing a PD-controller (outlined in 2.1) with a "fast" gain relative to the other inputs to track a desired pitch ϕ^*, and use the remaining "free" control affordance, u (2), to treat the COM as a fully-actuated particle on the xz plane.[7] It is then possible to track a pair of decoupled scalar velocity targets, $\dot{x}^*$ and $\dot{z}^*$ that "aim" the initial condition of the ensuing BF (ballistic flight) dynamics. The need for the horizontal velocity, $\dot{x}$, to track faster than the vertical velocity arises from the fact that once $\dot{z}$ is achieved, the normal forces required to slow down the second-order dynamical system will be negative, and thus violate the pinned-toe constraint. For this reason, we choose to servo a scalar double-integrator toward the target velocity in x, while tracking a constant acceleration in z. The advantage of such a formulation is twofold - it allows an estimation of stance time $t_{\text{stance}} \approx \frac{\dot{z}^*}{\ddot{z}^*}$, which provides a bound on the settling time for the velocity tracking in the horizontal degree of freedom, while simultaneously maximizing its affordance, which is bound by $||u_x|| \leq \mu||u_z||$. The control inputs are:

$$\begin{aligned} u_\phi &:= k_{p,\phi}(\phi^* - \phi) - k_d\dot{\phi} \\ u_x &:= k_{p,x}(\dot{x}^* - \dot{x}) \\ u_z &:= \ddot{z}^* \end{aligned} \tag{4}$$

DSG ends when the robot reaches the guard set $G_{\text{DSG,A}} \subset T\mathcal{Q}$, given by:

$$G_{\text{DSG,A}} := \left\{(q,\dot{q}) \in T\mathcal{Q} \middle| |(\phi^* - \phi)| < \epsilon_\phi, |(\dot{x}^* - \dot{x})| < \epsilon_x, |(\dot{z}^* - \dot{z})| < \epsilon_z \right\} \tag{5}$$

The subsequent aerial and landing modes can be combined into the reset map $R_{\text{DSG,DSS}} : G_{\text{DSG,A}} \to T\mathcal{Q}$, which assumes that the pitch remains nearly constant and that the appendages are held at constant extensions (r_f, r_r) and angles in the world frame $(\theta_{a,f}, \theta_{a,r})$. When landing, one of the following must occur: the back toe touches down first in mode (1,0); or the front toe touches down first in mode (0,2); or both toes touch simultaneously in mode (1,2). While a formal analysis is omitted, the assumption that the toe remains in contact after touchdown and the body rotates around the hip (θ_a remains constant) is made. Thus, the reset map as a function $q_r = R_{\text{DSG,DSS}}(q_{r,0})$, with the subcomponents x_r, x_f of q_r given from the corresponding components of $q_{r,0}$ is:

$$\begin{aligned} x_r &= x_{r,0} + \dot{x}_0 t_r, \quad \text{if} \quad t_r < t_f \\ x_f &= x_{f,0} + \dot{x}_0 t_f, \quad \text{if} \quad t_f < t_r \end{aligned} \tag{6}$$

[6] A simple heuristic might be to minimize the energy of the leap, and thus a user would select an attitude of ϕ_{max} and trajectory as near to optimal as the friction cone allows.

[7] While the basis of the "free" control inputs could be analytically developed and used to control the COM, we find it easier to perform a constrained optimization problem at each time step. This formulation explicitly enforces friction constraints, while guaranteeing the applied forces maintain the decoupling of the template models.

with

$$t_r = \frac{\dot{z}_0}{g} + \frac{\sqrt{\dot{z}_0^2 + 2g(z_{r,0} - r_r \cos\theta_{a,r})}}{g}$$
$$t_f = \frac{\dot{z}_0}{g} + \frac{\sqrt{\dot{z}_0^2 + 2g(z_{f,0} - r_f \cos\theta_{a,f} - L_1)}}{g} \tag{7}$$

Here, $\dot{z}_0$ is the vertical component of the body velocity at the beginning of the aerial mode, $z_{r,0}$ is the vertical position of the rear hip at that same time, and $z_{f,0}$ is a similar expression for the front hip. Adhering to the assumptions above, the final values of q can be determined from the kinematics as $\dot{q}$ goes to zero.

3.3 Dismounting Tasks

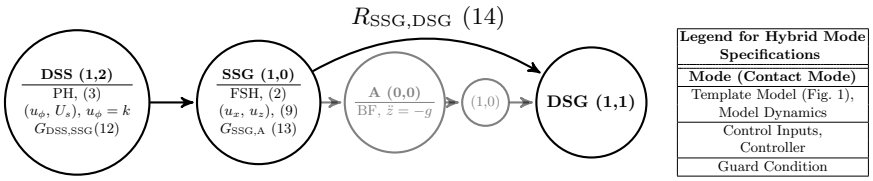

Fig. 4. A graph representing the hybrid dynamical system of the dismount behavior. The gravity driven aerial phase (A) and subsequent single stance landing mode (1,0) can be integrated out and included in the reset map $R_{\text{SSG,DSG}}$.

Dismounting tasks require that attention be paid to releasing the object without applying transverse forces, so that the object will not accelerate away from its original position during the maneuver. To do this, energy is injected via an open-loop pushing with the front legs, subject to the constraint that the ground reaction forces at the toe (GRF) are vertical. This condition is enforced by relating the available control inputs to the front appendage as follows:

$$u_{\theta_{a,f}} = -\frac{u_{r,f}}{r_f} \tan\theta_{a,f} \tag{8}$$

where $\theta_{a,f}$ is the front leg angle in the world frame. Once enforced, this controller can be applied at will, within saturation limits of the machine.

A necessary, albeit not sufficient condition derived from the dynamics in (2), informs the guard condition terminating mode DSS. This condition is derived from the need to ensure adequate normal forces are provided to maintain a pinned toe in the following phase. So while a force u_x is applied to the center of mass, the vertical applied force u_z must be $\frac{u_x}{\mu}$, where μ a conservative assumption made about the coefficient of friction between the toe and the environment, giving rise to a simple controller:

$$u_x = k u_z = \frac{k}{\mu} \tag{9}$$

Examining the forward kinmatics, the control inputs are:

$$\begin{aligned} u_{r,r} &= u_x \sin(\theta_{a,r}) - u_x \cos(\theta_{a,r}) \\ u_{\theta,r} &= -u_x r_r \cos(\theta_{a,r}) + \frac{u_x}{\mu} r_r \sin(\theta_{a,r}) \end{aligned} \tag{10}$$

Since the dismounting behavior occurs within a regime for which the values for θ_a are small, we get the following approximation of the front hip dynamics:

$$\begin{aligned} \ddot{z}_f &= -g + \frac{u_x(\kappa - 1)(1 + \theta_{a,r}^2 - 2\theta_{a,r}\mu)}{m_b \kappa \mu} + \mathcal{O}(\epsilon^2) \\ \ddot{x}_f &= \frac{u_x}{m_b} + \mathcal{O}(\epsilon^2) \end{aligned} \tag{11}$$

The system is energized maximally, as this equates to the furthest displacement in the following mode; however, we ensure that the maximum height of the object L_2 must not be exceeded by the front hip. Since $\theta_{a,r}$ will be strictly decreasing throughout the maneuver, (11) reveals that $\ddot{z}_f(t) \geq \ddot{z}_f(0), \forall t$. Thus a guard set that ensures that the height L_2 is not exceeded can be constructed as:

$$G_{\mathrm{DSS,SSG}} := \left\{ (q, \dot{q}) \in T\mathcal{Q} \middle| \dot{z}_f \leq \sqrt{2(L_2 - z_f)\ddot{z}_{f,0}^2} \right\} \tag{12}$$

The single-support mode, (SSG), implements the controller prescribed in the previous guard condition. Applying an open loop input u_x accelerates the front hip, per the template dynamics in (2), out of the volume enclosed by the previously gripped object. To maximize the performance, this constant acceleration is maintained until the front hip has reached its apex, described by the guard:

$$G_{\mathrm{SSG,A}} := \left\{ (q, \dot{q}) \in T\mathcal{Q} \middle| \dot{z}_f \leq 0 \right\} \tag{13}$$

This not only that the body rotation will keep the front hip away from the minimum lip height, but also it maximizes the flight time of the body in the subsequent aerial phase. This mode can be integrated out with the appropriate reset which locates the landing position of the rear toe as a function of the initial conditions of the aerial mode, described by $R_{\mathrm{SSG,DSG}} : G_{\mathrm{SSG,A}} \to T\mathcal{Q}$, such that the x_{RT} location of the toe for $q_{\mathrm{RT}} = R_{\mathrm{SSG,DSG}}(q_0)$ is given as follows:

$$x_{\mathrm{RT}} = \dot{x}_0 \sqrt{\frac{2}{g}(z_0 - r_r \cos\theta_{a,r})} \tag{14}$$

where $\dot{x}_0$ is the horizontal component of the COM velocity at the onset of the aerial phase, and z_0 is the vertical position of the body at that same time. The above leverages the assumptions that the back leg is held at fixed extension and angle in the world frame, and that the rotation of the body $\dot{\phi}$ is small. Once free of the grasping cage and ground contact is established and excess energy is damped out in mode DSG.

3.4 Leaping Tasks

The modes of the hybrid dynamical system governing "leaping" tasks are as follows: open loop energy injection in contact mode DSG (1,1), a leap in mode SSG (1,0), a short aerial mode A1, a pitch-stable, double-stance leap [18] in mode DSS (1,2), a second aerial mode (A2), and landing contact modes (2,0) and (0,2) which can be ignored by including their integrable, gravity-driven dynamics into the reset maps to be described later. We focus on the specific set of (robot, task, environment) triples defined by the "mismatch" between the robot's length and energy scales and the height of the ledge onto which it is leaping [29], where the environment requires a dynamic behavior to maneuver onto the object. Further restriction on this notion of mismatch requires that the robot utilize both of its sagittal plane actuators, while simultaneously minimizing the horizontal distance that the COM must travel.[8]

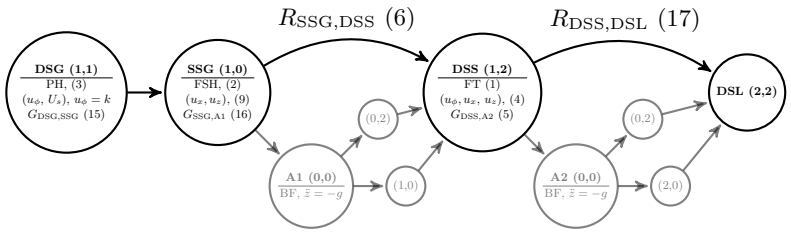

Fig. 5. A graph representing the hybrid dynamical system of the "leaping" behavior. This should be read in the sense of a "commutative diagram" (whereby any paths between the same pair of initial and final modes yield the same physical result) in that the gravity-driven modes (A1, A2, and the unnamed contact modes shown) have been integrated out in the reset maps $R_{\text{SSG,DSS}}$ (6) and $R_{\text{DSS,DSL}}$ (17).

Given a ledge, with parameters L_1, the ledge height, L_0, the distance of the ledge from the back toe , and L_2, the "limit surface" past which the robot will have overrun the viable landing surface on the object (Fig. 2), the goal is to generate a collection of task-targets ϕ^*_{DSS}, $\dot{x}^*_{\text{DSS}}$, and $\dot{z}^*_{\text{DSS}}$ for the mode DSS.

To accomplish the first of the sequential leaps, energy is injected in mode DSG, ensuring adequate front hip height z_f is achieved by designing $G_{\text{DSG,SSG}}$

$$G_{\text{DSG,SSG}} := \left\{ (q, \dot{q}) \in T\mathcal{Q} \middle| U_s(q, \dot{q}) \geq \ddot{z}_f L_1 + \frac{L_0}{u_x} \ddot{z}_f^2 \right\} \tag{15}$$

where L_0 is the distance the front hip must move to be over the edge of the ledge, u_x is a constant acceleration applied to the body in the subsequent mode, L_1 is the height of the ledge, U_s is the total energy of the system, and $\ddot{z}_f$ is a lower bound on $\ddot{z}_f(t)$ found by minimizing over the absolute leg angle, $\theta_{a,r}$.

[8] While this is a somewhat restrictive subset of the possible robot and environment pairings for this task, it does capture many of the most difficult real-world scenarios.

In mode SSG, the front hip is accelerated towards the ledge until it clears the edge, prescribing the guard $G_{\mathrm{SSG,A1}}$:

$$G_{\mathrm{SSG,A1}} := \left\{(q,\dot{q}) \in T\mathcal{Q} \middle| x_{FH} > L_0\right\} \tag{16}$$

where x_{FH} is the x-coordinate of the front hip. The rear toe can then be lifted and recirculated to neutral position, giving rise to an aerial phase, which is incorporated into reset map $R_{\mathrm{SSG,DSS}}$, of the same form as (6).

Upon the onset of contact mode DSS (1,2), a pitch target is chosen, by setting ϕ^*_{DSS} to value near the current $\phi(t)$. Then, the COM velocity is servoed to targets $\dot{x}^*_{\mathrm{DSS}}$, and $\dot{z}^*_{\mathrm{DSS}}$ to ensure that the trajectory at lift off carries the COM onto the ledge surface without overrunning it.[9] The guard set, $G_{\mathrm{DSS,A2}}$, is given in (5).

Upon termination of mode DSS the subsequent aerial and landing phases can be integrated out to landing at a given leg length as in (6), with:

$$\begin{aligned} t_r &= \frac{\dot{z}_0}{g} + \frac{\sqrt{\dot{z}_0^2 + 2g(z_{r,0} - r_r\cos\theta_{a,r} - L_1)}}{g} \\ t_f &= \frac{\dot{z}_0}{g} + \frac{\sqrt{\dot{z}_0^2 + 2g(z_{f,0} - r_f\cos\theta_{a,f} - L_1)}}{g}. \end{aligned} \tag{17}$$

4 Empirical Results

To facilitate the physical experiments, we have developed an open-source simulation package [30], based on ROS and Gazebo, that includes accurate kinematic and inertial descriptions of the Minitaur platform, along with the objects that Minitaur has to manipulate.[10] We overlay the simulation output (generated using exactly the same controller code as used in the physical experiments) on many of the empirical data plots of this section to emphasize the repeatable reliability of these closed loop behaviors as well as to give a sense of how effective the software package has proven in accelerating the debugging process.

4.1 Mounting Experiments

The efficacy of the mounting controller outlined in 3.2 is demonstrated on the Minitaur platform in a series of representative trials, demonstrating commonly used mounting behaviors from autonomous mobile-manipulation tasks, as well as unconventional behaviors that demonstrate the flexibility of the controller.

Mounting stools was a primary task in [3], and so we choose a representative situation in which the front hip is about a half body-length (0.2m) away from the

[9] Again, we avoid choosing a formulaic method for generating these velocity targets, and instead choose intuitively suitable targets to accomplish the task at hand.

[10] The package also includes various sensor descriptions, that can be used along with Minitaur for the simulations of different autonomous experiments (e.g., as those described in [4]). More importantly, the package acts as a software "bridge" between the ODE-based simulation [30] in Gazebo and proprietary software from Ghost Robotics [9], used for the control of the Minitaur platform.

center of the stool basin. We arbitrarily choose a set of velocities $(0.65, 1.5)$ that will cover that distance and not violate a friction cone constraint of $\mu = 0.5$ when pushing in the direction defined by them. In related future work, the authors of [3] hope to use a "cart"-like object, which while parametrically different from the stool, can be approached with the same mounting behavior. Here, the significant height of the "lip" of the cart requires a steeper trajectory to successfully clear it with the front toe. Furthermore, the larger squeezing pre-grasp cage volume provided by the larger lip feature allows us to jump further "into" the cart. The velocities $(0.65, 1.6)$ were chosen. An attitude of $+0.2$ radians was chosen to minimize energetic costs by minimizing the vertical distance the hip must travel to clear L_1. Fig. 6 shows the ground truth tracking of the body's COM and pitch provided by a Vicon motion tracking system. Five successive trials were performed for each program, totalling 15 trials, and all trials resulted in a successful capture of the target stool and cart. Snapshots of the trials are shown in Fig. 7.

4.2 Dismounting Experiments

To illustrate the dismounting behavior, three representative environments were chosen - a stool, a low cart, and a high cart. The maximum allowable height for each object was determined to be 0.47m, 0.54m, and 0.72m respectively, and given that that upper shanks of the Minitaur leg can protrude 0.1m above the hip, conservative height limits of 0.35m, 0.43m, and 0.55m where enforced in the guard condition described in (13). Again, five successive trials were performed on each of the three objects, each successful, and each with trajectory evaluated using ground truth from Vicon showing close agreement with the prescribed height in Fig. 8.

4.3 Leaping Experiments

To illustrate the leaping behavior, two representative environments were chosen - a low box ($L_1 = 0.22$m) and a high box ($L_1 = 0.32$m. The robot's back toe is placed 0.45m away from the ledge, in both cases. Per these initial conditions, a target velocity for the open-loop injection per (15) was found to be $1.0\frac{\text{m}}{\text{s}}$ and $1.0\frac{\text{m}}{\text{s}}$ for the respective tasks. In this case, each leap was chosen to track an $(\dot{x}, \dot{z})$ equal to $(0.9, 1.8)$ and $(1.1, 2.0)$, and ϕ that was 0.2rads less than the pitch at the onset of DSS. Each experiment was run five times to conform with previous experiments; however, while the Low Box trials yielded five successes on successive trials, the High Box trials had a single failure and thus that trial was thrown out. [11] The ground truth Vicon data are shown in contrast with the prescribed velocity targets for each task in Fig. 10.

[11] The authors suspect this is due to performance limits of the machine as the actuators were saturated in this more extreme case, and this failure is not representative of the repeatability of the method.

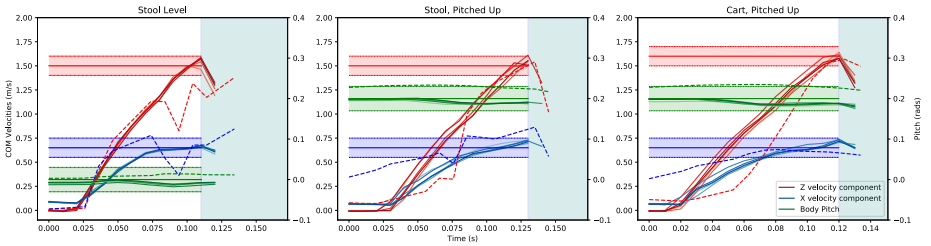

Fig. 6. The pitch, $\dot{x}$, and $\dot{z}$ during 15 trial leaps of representative stool and cart mounting tasks (plots display traces from five repetitions for each of three case instances). The shaded regions matching the color of the family of traces from each trial represent the basin for each task-target as described in (5). The dotted trajectories corresponding to each color are those from the simulation environment [30]. The cyan region indicates behavior termination.

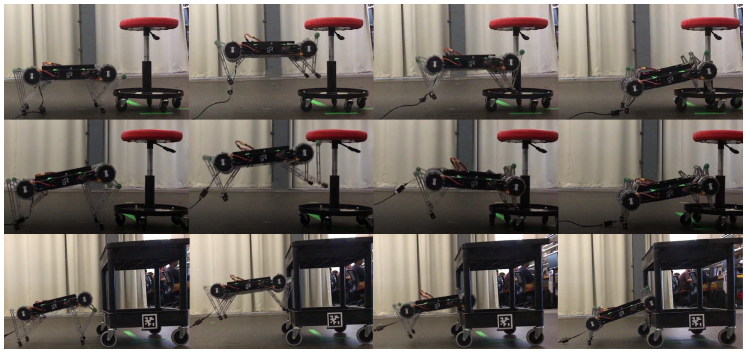

Fig. 7. A series of images from one of the trials of each of the mounting behaviors The top row is of a trial with a desired level pitch, the middle row is with a desired pitch of +0.2 radians, and the bottom row depicts a cart mounting task.

Acknowledgements

This work was supported in part by ONR grant #N00014-16-1-2817, a Vannevar Bush Fellowship held by the last author, sponsored by the Basic Research Office of the Assistant Secretary of Defense for Research and Engineering, and in part by AFRL grant FA865015D1845 (subcontract 669737-1).

References

1. J. E. Hopcroft, J. T. Schwartz, and M. Sharir, "On the Complexity of Motion Planning for Multiple Independent Objects; PSPACE-Hardness of the "Warehouseman's Problem"," *The International Journal of Robotics Research*, vol. 3, no. 4, pp. 76–88, 1984.

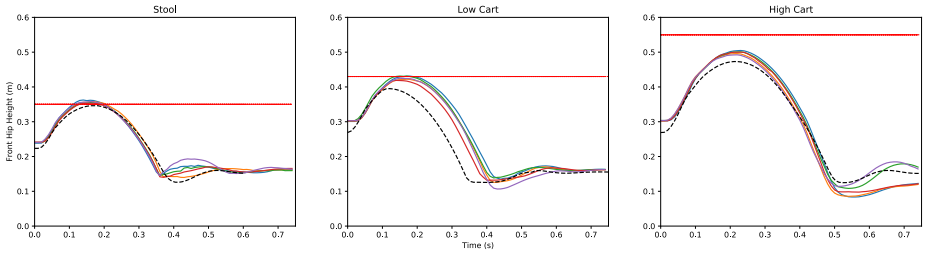

Fig. 8. The vertical trajectory of the front hip from 15 dismounting experiment trials, split across 3 different objects (plots display traces from five repetitions across each). The solid red line indicates the maximum allowable height encoded into the guard condition (13), and the black dotted trajectories are those from the simulation environment [30].

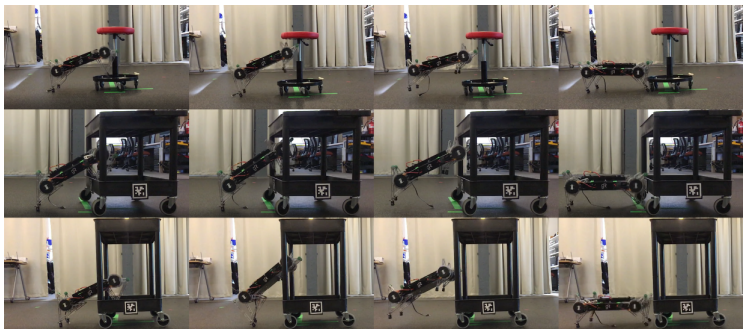

Fig. 9. A series of snap shots showing a sample dismounting behavior from each of the 3 distinct environments.

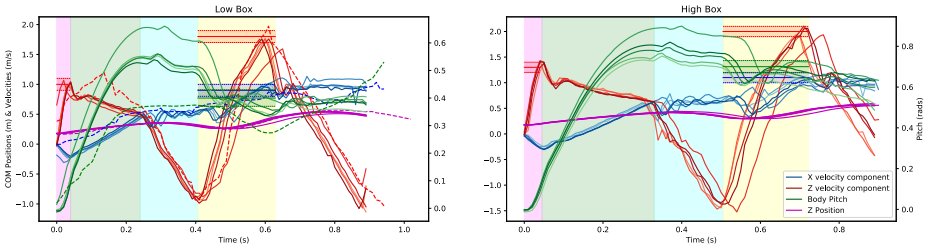

Fig. 10. The trajectories represent $\dot{x}$, $\dot{z}$, ϕ and z from 10 leaping experiment trials, across 2 boxes (plots display traces from five repetitions across each). The horizontal shaded regions matching the color of the family of traces from each trial represent the basin for each task-target as described in (15) and (5). The colored dotted trajectories are those from the simulation environment [30]. The vertical shaded regions separate the modes of the behavior, and were chosen by averaging the mode transition times of the five trials in each plot. Magenta is DSG, green is SSG, Cyan is A1, yellow is DSS and white is A2.

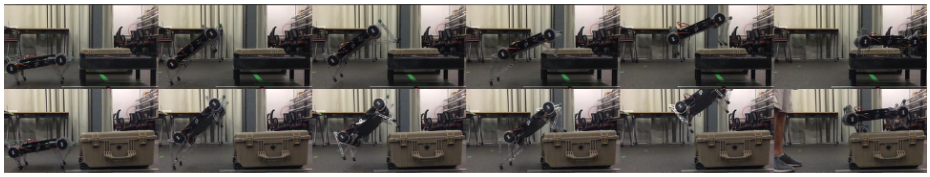

Fig. 11. A series of snapshots depicting each of the labeled modes from Fig. 5. The top row of images shows the low box, the bottom row shows the high box.

2. W. Vega-Brown and N. Roy, "Admissible Abstractions for Near-optimal Task and Motion Planning," in *27th International Joint Conference on Artificial Intelligence*, July 2018.
3. V. Vasilopoulos, W. Vega-Brown, O. Arslan, N. Roy, and D. E. Koditschek, "Sensor-Based Reactive Symbolic Planning in Partially Known Environments," in *IEEE International Conference on Robotics and Automation*, May 2018, pp. 5683–5690.
4. V. Vasilopoulos, T. T. Topping, W. Vega-Brown, N. Roy, and D. E. Koditschek, "Sensor-Based Reactive Execution of Symbolic Rearrangement Plans by a Legged Mobile Manipulator," in *IEEE/RSJ International Conference on Intelligent Robots and Systems*, 2018, pp. 3298–3305.
5. M. T. Mason, D. Pai, D. Rus, L. R. Taylor, and M. Erdmann, "A Mobile Manipulator," in *IEEE International Conference on Robotics and Automation*, vol. 3, May 1999, pp. 2322 – 2327.
6. M. T. Mason and K. M. Lynch, "Dynamic manipulation," in *IEEE/RSJ International Conference on Intelligent Robots and Systems*, 1993, pp. 152–159.
7. R. Full and D. Koditschek, "Templates and anchors: Neuromechanical hypotheses of legged locomotion on land," *Journal of Experimental Biology*, vol. 202, no. 23, pp. 3325–3332, 1999.
8. G. Kenneally, A. De, and D. E. Koditschek, "Design principles for a family of direct-drive legged robots," *IEEE Robotics and Automation Letters*, vol. 1, no. 2, pp. 900–907, 2016.
9. "Ghost Robotics," 2019. [Online]. Available: https://www.ghostrobotics.io
10. A. M. Johnson and D. E. Koditschek, "Toward a vocabulary of legged leaping," in *IEEE International Conference on Robotics and Automation*, 2013, pp. 2553–2560.
11. N. Koyachi, H. Adachi, M. Izumi, and T. Hirose, "Control of walk and manipulation by a hexapod with integrated limb mechanism: MELMANTIS-1," in *IEEE International Conference on Robotics and Automation*, vol. 4, 2002, pp. 3553–3558.
12. X. Ding and F. Yang, "Study on hexapod robot manipulation using legs," *Robotica*, vol. 34, no. 2, pp. 468–481, 2016.
13. B. U. Rehman, M. Focchi, J. Lee, H. Dallali, D. G. Caldwell, and C. Semini, "Towards a multi-legged mobile manipulator," in *IEEE International Conference on Robotics and Automation*, 2016, pp. 3618–3624.
14. M. Schwarz, T. Rodehutskors, D. Droeschel, M. Beul, M. Schreiber, N. Araslanov, I. Ivanov, C. Lenz, J. Razlaw, and S. Schller, "NimbRo Rescue: Solving Disaster-response Tasks with the Mobile Manipulation Robot Momaro," *Journal of Field Robotics*, vol. 34, no. 2, pp. 400–425, 2017.
15. L. Sentis and O. Khatib, "Synthesis of whole-body behaviors through hierarchical control of behavioral primitives," *International Journal of Humanoid Robotics*, vol. 2, no. 4, pp. 505–518, 2005.

16. R. Cisneros, K. Yokoi, and E. Yoshida, "Impulsive Pedipulation of a Spherical Object with 3D Goal Position by a Humanoid Robot: A 3D Targeted Kicking Motion Generator," *International Journal of Humanoid Robotics*, vol. 13, no. 2, 2016.
17. T. Strom-Hansen, M. Thor, L. B. Larsen, E. Baird, and P. Manoonpong, "Distributed Sensor-Driven Control for Bio-Inspired Walking and Ball Rolling of a Dung Beetle-Like Robot," in *SWARM*, 2017, pp. 196–199.
18. A. De, T. T. Topping, and D. E. Koditschek, "A Universal Template for Pitch-Steady Behaviors in Planar Floating-Torso Locomotion Models," *In Prep*, 2019.
19. ——, "Hybrid Averaging of Almost-Reversible Sagittal Hopping and Bounding Compositions," *In Prep*, 2019.
20. "Ghost Robotics Vision60," 2019. [Online]. Available: www.ghostrobotics.io/
21. G. Bledt, M. J. Powell, B. Katz, J. Di Carlo, P. M. Wensing, and S. Kim, "Mit cheetah 3: Design and control of a robust, dynamic quadruped robot," in *2018 IEEE/RSJ International Conference on Intelligent Robots and Systems (IROS)*, Oct 2018, pp. 2245–2252.
22. A. Robotics, "Cassie," 2019. [Online]. Available: www.agilityrobotics.com
23. B. Dynamics, "Spot-mini," 2019. [Online]. Available: www.bostondynamics.com
24. G. Konidaris, L. P. Kaebling, and T. Lozano-Perez, "From Skills to Symbols: Learning Symbolic Representations for Abstract High-Level Planning," *Journal of Artificial Intelligence Research*, vol. 61, pp. 215–289, 2018.
25. A. M. Johnson, S. A. Burden, and D. E. Koditschek, "A hybrid systems model for simple manipulation and self-manipulation systems," *The International Journal of Robotics Research*, vol. 35, no. 11, pp. 1354–1392, 2016.
26. A. Rodriguez, M. T. Mason, and S. Ferry, "From caging to grasping," *The International Journal of Robotics Research*, vol. 31, no. 7, pp. 886–900, 2012.
27. A. De and D. E. Koditschek, "Vertical hopper compositions for preflexive and feedback-stabilized quadrupedal bounding, pacing, pronking, and trotting," *The International Journal of Robotics Research*, vol. 37, no. 7, pp. 743–778, Jun 2018.
28. M. Vahedi and A. Van Der Stappen, "Caging polygons with two and three fingers," *Springer Tracts in Advanced Robotics*, vol. 47, pp. 71–86, 2008.
29. T. T. Topping, G. Kenneally, and D. E. Koditschek, "Quasi-static and dynamic mismatch for door opening and stair climbing with a legged robot," in *IEEE International Conference on Robotics and Automation*, May 2017, pp. 1080–1087.
30. "`ghost_gazebo`: ROS package for the simulation of Ghost Robotics platforms using Gazebo," 2019. [Online]. Available: https://github.com/KodlabPenn/ghost_gazebo/